12-22-2005

Analysis of Binary Adsorption of Polar and Nonpolar Molecules in Narrow Slit-Pores by Mean-Field Perturbation Theory

R. R. Kotdawala

Nikolaos Kazantzis
Worcester Polytechnic Institute, nikolas@wpi.edu

Robert W. Thompson
Worcester Polytechnic Institute, rwt@wpi.edu

Analysis of binary adsorption of polar and nonpolar molecules in narrow slit-pores by mean-field perturbation theory

R. R. Kotdawala, Nikolaos Kazantzis, and Robert W. Thompson[a)]
Department of Chemical Engineering, Worcester Polytechnic Institute, Worcester, Massachusetts 01609

(Received 6 June 2005; accepted 11 October 2005; published online 30 December 2005)

In the present research study, we present the development of a model for predicting the adsorption of binary mixtures of nonpolar molecules, as well as polar molecules, based on density functional theory with mean-field approximation in narrow slit-pores. The first system under consideration is comprised of a binary mixture of nonpolar molecules, modeled by considering intermolecular dispersion forces, whereas the second system comprised of a binary mixture of polar molecules is modeled by considering orientation averaged electrostatic interactions, namely dipole-dipole and dipole-induced dipole interactions as well as dispersion interactions. An explicit equation for the Helmholtz free energy of the pore phase binary fluid mixture is derived. The proposed model is used to simulate the selective sorption of ethane from an ethane-methane mixture and water from a methanol-water mixture in the slit-pore. The simulated results are interpreted by studying the relative contributions of fluid-wall and fluid-fluid interactions. Finally, simulation results obtained are compared with the results of existing models and molecular simulations in the literature.
 [DOI: 10.1063/1.2133736]

I. INTRODUCTION

The adsorption of fluid mixtures in microporous materials is a frequently encountered process in natural gas purification, and in the design of porous polymeric membranes in fuel cells. In the case of natural gas purification, methane is separated from the hydrocarbon mixture containing ethane, propane, and butane as well. Even though some experimental data are available for sorption of the binary mixtures of methane with ethane, propane, and butane,[1–4] very few studies based on molecular theory have been carried out.[5–8] Tan and Cracknell[5,6,9,10] addressed the effect of pore size, operating pressure, temperature on the selectivity of ethane over methane in methane-ethane mixtures using nonlinear mean field theory (NLMFT) and Grand Canonical Monte Carlo (GCMC) simulations, respectively. Jiang *et al.*[7] studied the influence of pore width, intermolecular potential parameters and state conditions on the selective adsorption of trace components like propane in methane, butane in methane, and nitrogen in methane using NLDFT. Davies *et al.*[11] also predicted adsorption equilibrium data for methane-ethane mixtures in activated carbon by combining pore size distribution and GCMC simulations, and compared their results with existing experimental data.

Moreover, in light of the above considerations, further systematic studies on sorption of methanol, water, and methanol-water mixtures are required to characterize proton exchange membranes (PEMs) for designing efficient PEM fuel cells,[12–17] and in the dehydration process of methanol manufacturing.[18,19] However, while numerous experimental studies have been carried out on this system,[12,13,18–20] to the best of our knowledge, only a few simulation results[21,22] based on molecular theory have been reported in the literature. Shevade *et al.*[21,22] simulated water-methanol mixture sorption in slit shaped graphite and silicalite pores, with and without acidic sites, using GCMC simulations to explain complex water-methanol mixture behavior.

Only a few attempts have been made to apply density functional/perturbation theory for studying binary mixtures of nonpolar molecules[5–8,25] and to our knowledge, no attempt has been made to apply these theories to a mixture of polar molecules. In the present work, we extend the single component mean-field perturbation theory reported by Schoen and Diestler[23] and Kotdawala *et al.*[24] for studying the sorption of binary mixtures of methane-ethane (nonpolar molecules) and methanol-water mixtures (polar molecules) in slit shaped pores. For modeling the nonpolar system, we consider standard LJ intermolecular potentials to account for dispersion forces, while in the case of the polar system, we consider orientation dependent dipole-dipole and dipole-induced dipole intermolecular potentials to account for electrostatic interactions in addition to dispersion interactions. In order to explicitly derive an analytical equation/expression for the Helmholtz free energy of the thermodynamic system under consideration, we need to use intermolecular potentials for orientationally dependent interactions which are in the form of orientation independent intermolecular potentials. This can be achieved by using the statistical averaging method recently adopted by Kotdawala *et al.*[24]

II. MODEL DEVELOPMENT

Consider two different fluids confined in the slit-pore, of width s_Z and area A, shown in Fig. 1.

The partition function for the two component system is given by[25]

[a)]Electronic mail: rwt@wpi.edu

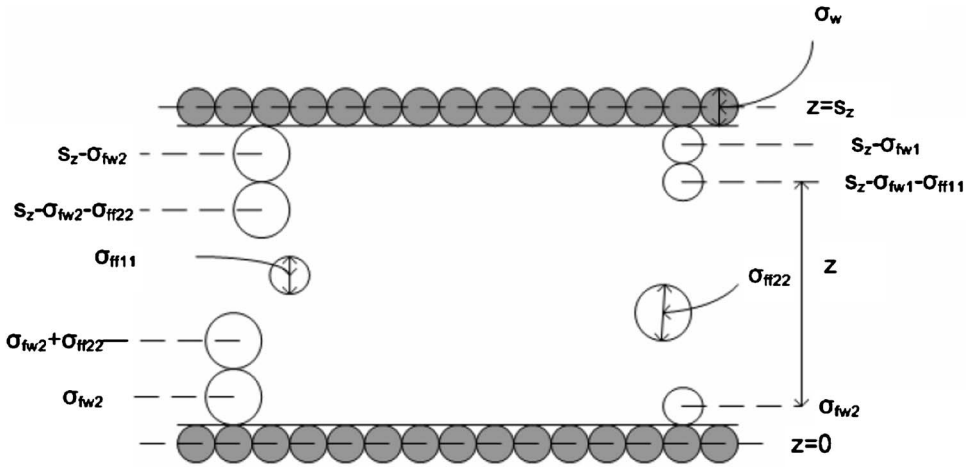

FIG. 1. Side view of the slit-pore model showing wall atoms and fluid molecules

$$Q = \frac{Z_N}{N_1!\,N_2!\,\lambda_1^{3N_1}\lambda_2^{3N_2}}, \tag{1}$$

where Z_N is the associated configuration integral, N_1 and N_2 are the number of molecules of components 1 and 2, respectively, 1 and 2 are thermal wavelengths of components 1 and 2,[23,24] and

$$Z_N = \int d\omega_1^{N_1} \int dr_1^{N_1} \int dr_2^{N_2} \int d\omega_2^{N_2} \exp(-\beta U_c), \tag{2}$$

where, $\beta = 1/kT$ and U_c is the configuration internal energy of the system, which is defined as follows:

$$U_c = U_c{}^0 + U_c'. \tag{3}$$

In the above expression U_c^0 is the configuration energy of the reference (nominal) system, and U_c' is the configuration energy of the system perturbed from the above nominal one.

The configuration integral can be conveniently calculated by identifying the following two parts:

$$Z^0 = \int d\omega_1^{N_1} \int dr_1^{N_1} \int dr_2^{N_2} \int d\omega_2^{N_2} \exp(-\beta U_c^0) \tag{4}$$

which is the configuration integral associated with the reference system, and

$$Z^P = \int d\omega_1^{N_1} \int dr_1^{N_1} \int dr_2^{N_2} \int d\omega_2^{N_2} \exp(-\beta U'_c) \tag{5}$$

which is the configuration integral associated with the perturbation from the above reference system.

Note that the mean-field configuration integral can be approximated by[23]

$$Z_N = \exp(-\beta \langle U'_c \rangle), \tag{6}$$

where

$$\langle U'_c \rangle = \langle U'_{11f} \rangle + \langle U'_{22f} \rangle + \langle U'_{12f} \rangle + \langle U'_{1fw} \rangle + \langle U'_{2fw} \rangle. \tag{7}$$

In the above expression $\langle U'_{11f} \rangle$ is associated with the fluid-fluid interactions pertaining to component 1, $\langle U'_{22f} \rangle$ is associated with the fluid-fluid interactions pertaining to component 2, $\langle U'_{12f} \rangle$ is associated with the fluid-fluid interactions pertaining to component 1 and component 2, $\langle U'_{1fw} \rangle$ is associated with the fluid-wall interactions between component 1 and the pore wall, and $\langle U'_{2fw} \rangle$ is associated with the fluid-wall interactions between component 2 and the pore wall.

A. Model equations for binary mixture of nonpolar gases

The overall configuration energy accounts for the following intermolecular energy terms:

(1) The fluid-fluid interactions associated with components i and j (Ref. 23),

$$U'_{ijf}(r) = -4\varepsilon_{ffij}\left(\frac{\sigma_{ffij}^6}{r^6}\right), \quad \text{where } i,j = 1,2, \tag{8}$$

where, σ_{ffij} is the collision diameter of component i and j and r is the distance between two molecules i and j. Note that ε_{ffij} is the fluid-fluid interaction parameter for component i and component j.

The average value of $U'_{11f}(r)$ for a slit-pore geometry is obtained by a method of integration introduced by Schoen and Diestler,[23] and later used by Kotdawala *et al.*,[24]

$$\langle U'_{11f} \rangle = a_{p1} N_1 \rho_{p1}, \tag{9}$$

where the pore density of component 1 is given by

$$\rho_{p1} = \frac{N_1}{A s_z}, \tag{10}$$

$$a_{p1} = a_{b1}\left[1 - \left(\frac{\frac{3\sigma_{ff11}}{\sigma_{fw1}}}{4(\xi_1 - 2)}\right) + \left(\frac{\frac{\sigma_{ff11}^3}{\sigma_{fw1}^3}}{8(\xi_1 - 2)^3}\right)\right] \tag{11}$$

with

$$\xi_1 = \frac{s_z}{\sigma_{fw1}}, \tag{12}$$

$$\sigma_{fw1} = (\sigma_{ff11}\sigma_w)^{1/2}, \tag{13}$$

where, σ_w is the effective diameter of the atom of pore wall, and

$$a_{b1} = \frac{8\pi\varepsilon_{ff11}\sigma_{ff11}^3}{3}. \tag{14}$$

Similarly, the average fluid-fluid interactions associated with component 2 (Ref. 23) can be given by

$$\langle U'_{22f}\rangle = a_{p2}N_2\rho_{p2}. \tag{15}$$

An explicit characterization of the various terms in Eq. (15) is given in the Appendix [Eqs. (A1)–(A5)].

The average value of fluid-fluid interactions associated with component 1 and component 2 $[U'_{12f}(r)]$ for a slit-pore geometry is given by

$$\langle U'_{12f}\rangle = a_{p12}N_1\rho_{p1}. \tag{16}$$

Similarly, an explicit characterization of the various terms in Eq. (16) is given in the Appendix [Eqs. (A6)–(A10).

(2) The fluid-wall interactions between component i and the pore wall can be expressed mathematically as follows:[23]

$$U'_{ifw} = \frac{-2\pi\rho_w\varepsilon_{fwi}\sigma_{fwi}^6}{3d}[z_i^{-3} + (s_z - z_i)^{-3}], \quad \sigma_{fwi} \leqslant z_i \leqslant s_z - \sigma_{fwi},\ i = 1,2. \tag{17}$$

Here, $\varepsilon_{ifw} = (\varepsilon_{fij}\varepsilon_w)^{1/2}$, $i = 1,2$ ρ_w is the aerial density of the solid substrate, and d is the distance between two wall atoms.

The average value of U'_{1fw} is given by[23,24]

$$\langle U'_{1fw}\rangle = \psi_1(\xi_1) = \frac{2N\pi\rho_w\varepsilon_{fwl}\sigma_{fwl}^3}{3d(\xi_1 - 1)}\left(\frac{1}{(\xi_1 - 1)^2} - 1\right), \quad \xi_1 > 2. \tag{18}$$

Similarly, the average value of U'_{2fw} is given by[23,24]

$$\langle U'_{2fw}\rangle = \psi_2(\xi_2) = \frac{2N\pi\rho_w\varepsilon_{fw2}\sigma_{fw2}^3}{3d(\xi_2 - 1)}\left(\frac{1}{(\xi_2 - 1)^2} - 1\right), \quad \xi_2 > 2. \tag{19}$$

B. Model equations for binary mixtures of polar molecules

In the case under consideration, the configuration energy accounts for the following intermolecular energy terms:

(1) The fluid-fluid interactions associated with component 1 are represented by[24,26–29]

$$U'_{ijf}(r) = \left[-\frac{1}{(4\pi\varepsilon_0)^2 r^6}\left(\frac{3\alpha_i\alpha_j(I_i + I_j)}{I_i I_j 4}\right)\right] - \frac{1}{(4\pi\varepsilon_0)^2 r^6}\left(\frac{\mu_i^2\mu_j^2}{3KT} + \mu_i^2\alpha_i + \mu_j^2\alpha_j\right), \tag{20}$$

where, $i = 1,2$.

In the above expression, μ_i and μ_j are the permanent dipole moment of component i and j, respectively, α_i and α_j are the average polarizibility of component i and component j, respectively, I_i and I_j are the first ionization potential of component i and j, respectively, and r is the distance between molecules i and j. Notice that the first term in Eq. (20) accounts for the dispersion interactions and the second term accounts for the angle independent electrostatic interactions obtained through a statistical averaging method.[24,26] The first term in the second large parentheses in Eq. (20) accounts for dipole-dipole interactions and the other terms account for dipole-induced dipole interactions.

The average value of the interaction energy can be obtained by integrating Eq. (20) over the pore dimensions, as shown by Kotdawala *et al.*,[24] leading to the following expression:

$$\langle U'_{11f}\rangle = a_{p11}N_1\rho_{p1}, \tag{21}$$

where

$$a_{p11} = \frac{4\pi a_{p1}}{3\sigma_{ff11}^3(s_z - 2\sigma_{fw1})}\left(-\frac{3}{2}\sigma_{ff11} + 2(s_z - 2\sigma_{fw1}) + \frac{\sigma_{ff11}^3}{4(s_z - 2\sigma_{fw1})^2}\right), \tag{22}$$

$$a_{p1} = \frac{1}{(4\pi\varepsilon_0)^2}\left[\left(\frac{2\mu_1^4}{3kT}\right) + 2\mu_1^2\alpha_1 + \left(\frac{3\alpha_1^2 I_1}{4}\right)\right]. \tag{23}$$

Similarly, the average value of the fluid-fluid interaction energy for component 2 can be given by

$$\langle U'_{22f}\rangle = a_{p22}N_2\rho_{p2}. \tag{24}$$

Notice that an explicit characterization of the various terms in Eq. (24) is given in the Appendix [Eqs. (A11) and (A12)].

The average fluid-fluid interactions between components 1 and 2 are given by the expression below,

$$\langle U'_{12f}\rangle = a_{p121}N_1\rho_{p1}. \tag{25}$$

An explicit characterization of the various terms in Eq. (25) is given in the Appendix [Eqs. (A13) and (A14)].

(2) Finally, the fluid-wall interactions for component i and the wall can be calculated from Eq. (17). Therefore, $\langle U'_{1fw}\rangle$ can be calculated through Eq. (18) and $\langle U'_{2fw}\rangle$ through Eq. (19).

C. Helmholtz free energy and chemical potential for pore and bulk phases

The Helmholtz free energy can be calculated as follows:[23]

$$F = -\beta^{-1}\ln(Q) \tag{26}$$

$$= -\beta^{-1}\ln\left(\frac{Z^0\langle\exp(-\beta U'_c)\rangle}{N_1!\,N_2!\,\lambda_1^{3N_1}\lambda_2^{3N_2}}\right) \tag{27}$$

$$= -\beta^{-1}\ln\left(\frac{Z^0}{N_1!\,N_2!\,\lambda_1^{3N_1}\lambda_2^{3N_2}}\right) - \beta^{-1}\ln[\langle\exp(-\beta U'_c)\rangle] \tag{28}$$

$$= -\beta^{-1} \ln\left(\frac{Z^0}{N_1!\,N_2!\,\lambda_1^{3N_1}\lambda_2^{3N_2}}\right) + \langle U'_c \rangle. \tag{29}$$

Note that[23]

$$Z^0 = (As_z - N_1 b p_1 - N_2 b p_2)^{N_1+N_2}, \tag{30}$$

where

$$b_{p1} = \frac{8\pi\sigma_{ff11}^3}{3} \tag{31}$$

and

$$b_{p2} = \frac{8\pi\sigma_{ff22}^3}{3}. \tag{32}$$

Combining Eqs. (9), (15), (16), (18), and (19) or Eqs. (21), (24), (25), and (18) and (19) with (7) and (29), one obtains the following expression for the Helmholtz free energy associated with the pore phase:

$$F_p = \frac{-(N_1+N_2)}{\beta}[\ln(As_z - N_1 b p_1 - N_2 b p_2)] + \ln N_1! + \ln N_2! + N_1 \ln \lambda_1 + N_2 \ln \lambda_2 - N_1\psi_1 - N_2\psi_2 - N_1 a_{p1}\rho_{p1} - N_2 a_{p2}\rho_{p2} - N_1 a_{p121}\rho_{p1}. \tag{33}$$

Similarly, the Helmholtz free energy, F_b for the bulk phase is given by the following:

For $\rho_{b2} < \rho_{b1}$,

$$F_b = \frac{-(N_1+N_2)}{\beta}[\ln(As_z - N_1 b_{b1} - N_2 b_{b2})] + \ln N_1! + \ln N_2! + N_1 \ln \lambda_1 + N_2 \ln \lambda_2 - N_1 a_{b1}\rho_{b1} - N_2 a_{b2}\rho_{b_2} - N_2 a_{b12}\rho_{b2}. \tag{34}$$

For $\rho_{b1} < \rho_{b2}$,

$$F_b = \frac{-(N_1+N_2)}{\beta}[\ln(As_z - N_1 b_{b1} - N_2 b_{b2})] + \ln N_1! + \ln N_2! + N_1 \ln \lambda_1 + N_2 \ln \lambda_2 - N_1 a_{b1}\rho_{b1} - N_2 a_{b2}\rho_{b2} - N_1 a_{b121}\rho_{b1}, \tag{35}$$

where, for polar molecules, a_{b1}, a_{b2}, and a_{b121} are

$$a_{b1} = \frac{4\pi a_{p1}}{3\sigma_{ff11}^3}, \tag{36}$$

$$a_{b2} = \frac{4\pi a_{p2}}{3\sigma_{ff22}^3}, \tag{37}$$

$$a_{b121} = \frac{4\pi a_{b12}}{3\sigma_{ff12}^3}. \tag{38}$$

Note that for nonpolar molecules, a_{b1}, a_{b2}, and a_{b121} are given by Eqs. (14), (A3), and (A7).

Furthermore, at equilibrium, the chemical potentials of bulk and adsorbed phases are equal, thus

$$\mu_{P1} = \mu_{b1}, \tag{39}$$

$$\mu_{P2} = \mu_{b2}. \tag{40}$$

D. Equilibrium pore densities in the low pressure regime

Note that at low pressures, fluid-fluid interactions can be ignored, and therefore, the equilibrium density for component 1 in the pores is given by[5,6]

$$\rho_{p1} = \rho_{b1} \exp(-\psi_1/kT) \tag{41}$$

while the equilibrium density for component 2 in the pores is given by[5,6]

$$\rho_{p2} = \rho_{b2} \exp(-\psi_2/kT). \tag{42}$$

E. Equilibrium pore densities in the moderate to high pressure regime

Fileti *et al.*[30] showed through *ab initio* calculations that the dipole moments of methanol and water monomers are 1.71D and 1.88 D and 2.49 D and 2.91 D for dimers. Water and methanol generally exist as monomers in vapor phase, while in the liquid phase they are typically found in the form of dimers. Water and methanol might exist as a vapor or liquid in the pore depending on the external pressure, temperature, and fluid-wall interactions. In that case it would be convenient to consider the dipole moment variations with respect to pore densities. In the absence of information about the exact relationship between the dipole moment and pore densities, a linear relationship between the two variables was assumed. We assigned 1.71 D to the vapor phase density of methanol and 2.49 D to liquid phase density of methanol at normal temperature and pressure and a linear fit was performed in the following fashion:

$$D_{\text{methanol}} = C_2\rho_{p2} + X_2. \tag{43}$$

The dipole moment variations for water were fitted in a similar manner, yielding

$$D_{\text{water}} = C_1\rho_{p1} + X_1. \tag{44}$$

The values of C_1, C_2, X_1, and X_2 are the respective slopes and intercepts of the above linear fits. Therefore, the equilibrium density profile can be obtained by solving the systems of algebraic Eqs. (39), (40), (43), and (44) simultaneously.

III. RESULTS AND DISCUSSION

A. Selectivity of component 2 over component 1

Selectivity, S, of component 2 over 1 can be defined as follows:[5,6]

$$S = \frac{x_{p2}/x_{p1}}{y_{b2}/y_{b1}}, \tag{45}$$

where, x_{p2} and x_{p1} represent the mole fraction of component 1 and 2, respectively, in the pore phase, while y_{b2} and y_{b1} are the mole fractions of components 1 and 2 in the bulk phase. Alternatively, we may define the selectivity as follows:

$$S = \frac{\rho_{p2}/\rho_{b2}}{\rho_{p1}/\rho_{b1}}. \tag{46}$$

The following parameter values were used in all simulation runs for the methanol-water system under consideration:

(1) Fluid-fluid interactions.

Component	Component name	I (eV)	$\alpha\times10^{24}$ (cm^3)	μ (Debye)
1	Water	12.6	1.5	1.9
2	Methanol	10.7 (Ref. 31)	3.4 (Ref. 28)	1.7 (Ref. 28)

(2) Fluid-wall interactions.

Component	ϵ(kJ/mol)	σ(Å)
Water (Ref. 32)	0.6485	3.11
Methanol	0.7887	3.4225
Carbon (Ref. 5)	0.2328	3.4

Methanol molecule parameters were obtained from Shevade *et al.*[21,22] by averaging the values of the atoms that form the methanol molecule.

The following parameter values were used in the simulation runs for the methane-ethane system of interest:[5,6]

Component	Component name	ϵ(kJ/mol)	σ(Å)
1	Methane	1.22	3.81
2	Ethane	2.01	3.95
	Carbon (Ref. 21)	0.2328	3.4

B. Comparison with ideal adsorption solution theory (IAST)[33,34]

IAST[33,34] represents essentially an application of Raoult's law to adsorbed phases. It can be used to predict the behavior of binary component adsorption systems by a methodological reduction technique that uses two single component adsorption systems.[33,34] For a given component i, one can write

$$Py_i = P_i^0(\pi)x_i, \tag{47}$$

where y_i and x_i are the bulk and pore mole fractions of component i, respectively, P is the total bulk pressure, and $P_i^0(\pi)$ is the bulk pressure corresponding to the spreading pressure π in the component isotherm of component i. For a pore width of 9.7 and 15.4 Å , we used the mean field theory[23] for methane and ethane for which P_i^0 and π are related according to the following formula:

$$\pi(P_i^0) = \frac{RT}{A}\int_0^{P_i^0} n_i^0(p)d\ln p. \tag{48}$$

It is possible, for example, to calculate x_i for a given P and y_i by first solving for $P_i^0(\pi)$ in the equation

$$\sum_i \frac{Py_i}{P_i^0(\pi)} - 1 = 0. \tag{49}$$

This equation follows from (47), since the sum of the mole fractions in the pore must equal unity. We used Unilan equation[30] to fit the single component data obtained from the simulation studies.

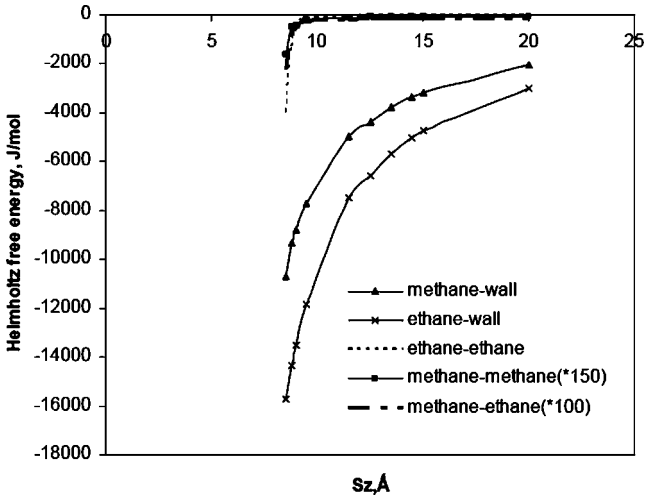

FIG. 2. Relative magnitudes of methane-wall, ethane-wall, ethane-ethane, methane-methane (×150), and methane-ethane (×100) interactions as a function of pore width for $y_{b1}=0.9$ (methane) at 280 K.

C. Comparisons with the results of Tan (Refs. 5 and 6) and Shevade *et al.* (Refs. 21 and 22)

In order to compare our simulation results with Tan[5,6] and Shevade *et al.*,[21,22] we replaced the fluid-wall intermolecular potential in Eq. (17) with the following intermolecular potential expressions.

The fluid-wall interactions between component i and the pore wall are represented as follows:[5,6]

$$U'_{ifw}(z) = \varepsilon_{wi}\left[2/5(\sigma_{fwi}/z)^{12} - (\sigma_{fwi}/z)^4 - \left(\frac{\sigma_{fwi}^4}{3s_z(z+0.61s_z)^3}\right)\right], \tag{50}$$

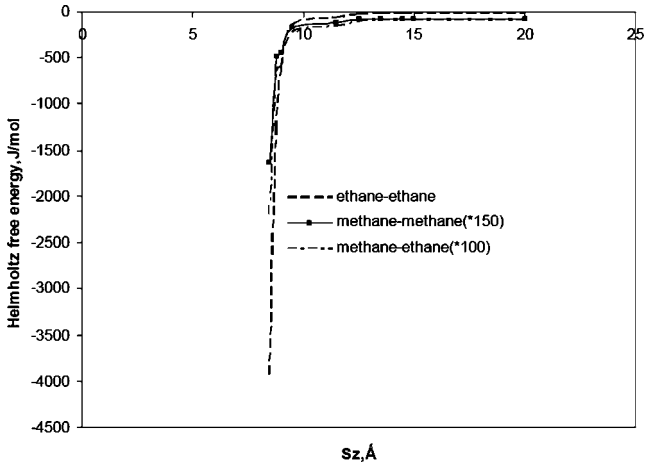

FIG. 3. Relative magnitudes of ethane-ethane, methane-methane (×150), and methane-ethane (×100) interactions as a function of pore width for $y_{b1}=0.9$ (methane) at 280 K.

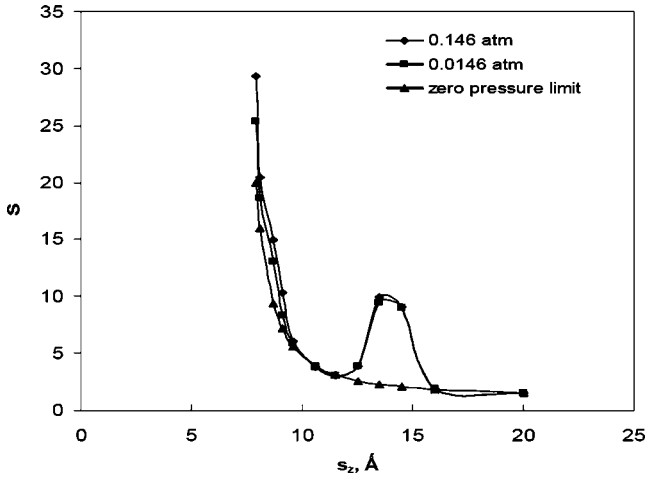

FIG. 4. Selectivity of ethane over methane as a function of pore size at 280 K and $y_{b1}=0.1$ (methane). Results shown for operating pressures in the limit of zero pressure to 0.146 atm.

$$\varepsilon_{wi} = 2\pi\rho_s\varepsilon_{fwi}\sigma_{fwi}^2 s_z, \quad i = 1,2, \tag{51}$$

where, ρ_s is the aerial density of the solid substrate, ε_{fwi} is fluid-wall interaction parameter for component i, and fwi is the effective fluid-wall collision diameter for component i. Then, the average value of $U'_{ifw}(z_i)$ is given by

$$\psi_i = \int_0^{s_z} U'_{ifw}(z) + U'_{ifw}(s_z - z)dz = \langle U'_{ifw} \rangle. \tag{52}$$

D. Methane-ethane mixtures

Figure 2 shows how the relative contributions of the fluid-wall (methane-wall and ethane-wall) interactions and fluid-fluid (methane-methane, methane-ethane, and ethane-ethane) interactions change as a function of pore size. The figure indicates that the fluid-wall interactions dominate over fluid-fluid interactions, due to weaker fluid-fluid dispersion interactions attributed to the nonpolar nature of methane and ethane. In the pore size range of 10 Å or greater, the magnitudes of fluid-fluid interactions are less than 100th of the fluid-wall interactions, which suggests that adsorption is mainly governed by fluid-wall interactions. From Fig. 2, it is difficult to compare fluid-fluid interactions between ethane-ethane, ethane-methane, and methane-methane. Figure 3 shows that the magnitudes of interactions between methane-ethane and methane-methane are almost the same because of the small differences in molecular sizes and the LJ interaction parameter. However, the ethane-ethane interactions are almost 100 times greater than those of methane-methane and methane-ethane due to the higher density of ethane molecules within the pore.

Figure 4 shows the selectivity calculated using Eq. (46). As the pore size decreases, the selectivity for ethane increases due to increased fluid-wall interactions, which favor ethane (Fig. 2). The selectivity at pressures of 0.0146 and 0.146 atm show different behavior. The selectivity decreases due to molecular sieving effects and contact layer formation from pore size of 7.8 to 12.5 Å and again increases with pore sizes up to 14.5 Å due to space available for ethane molecules to enter into the pore. Above 14.5 Å selectivity decreases due to molecular sieving effects and weak fluid-wall interactions in large pores.

In order to test the sensitivity of the proposed model to the temperature, the selectivity was simulated as a function of temperature. Results in Fig. 5 show that the selectivity decreases as temperature increases due to the high kinetic energy of the molecules, in the range of 3–5 kJ/mol.

Figure 6 shows that the ethane selectivity increases as the pressure increases from zero, due to increased fluid-wall interactions in the monolayer, in the range of 6–12 kJ/mol. However, S then decreases, because of the completion of monolayer formation, which results in weak fluid-fluid interactions in the range of 0.2–0.5 kJ/mol.

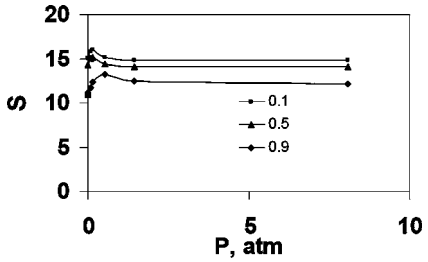

FIG. 6. Selectivity of ethane over methane as a function of operating pressure for 10 Å pore size at 280 K. Results shown for $y_{b1}=0.9$, 0.5, and 0.1 (methane).

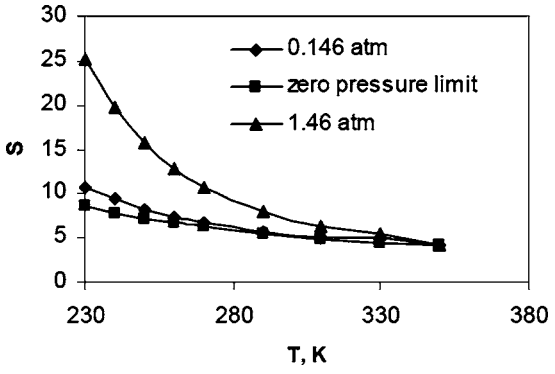

FIG. 5. Selectivity of ethane over methane as a function of temperature for 9.5 Å pore size at $y_{b1}=0.5$ (methane). Results shown for operating pressures in the limit of zero pressure to 1.46 atm.

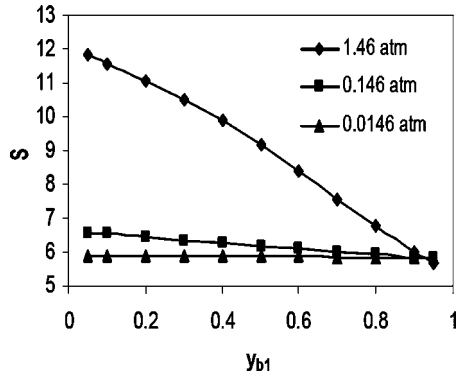

FIG. 7. Selectivity of ethane over methane as a function of bulk methane mole fraction (y_{b1}) for 13 Å pore size at 280 K. Results shown for operating pressures of 0.0146, 0.146, and 1.46 atm.

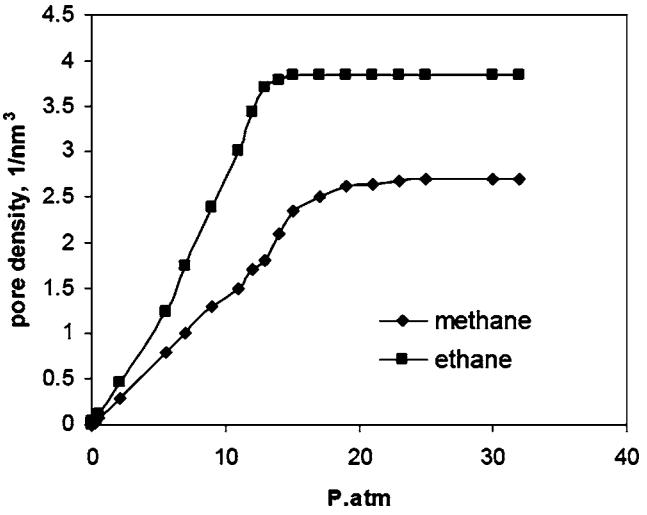

FIG. 8. Pore densities of methane and ethane as a function of operating pressure for 9.7 Å pore width at 286 K.

Figure 7 shows the ethane selectivity as a function of bulk mole fraction of methane at three different pressure values, 0.0146, 0.146, and 1.46 atm at 280 K for a 13 Å pore size. The selectivity decreases as the methane concentration increases in the bulk phase. The selectivity was found to be more sensitive to methane bulk mole fraction at higher pressures due to enhanced ethane-wall interactions as compared to lower pressures.

In order to compare the simulated results from the proposed model with the predictions from IAST and results from Tan *et al.*, we simulated single component isotherms of methane and ethane for the pore size of 9.7 Å at 286 K which were obtained by using mean-field theory.[23] The single component isotherms were fitted using the UNILAN equation and applying IAST[33,34] for binary component systems and are shown in Fig. 8.

Figure 9 shows the comparison of the selectivity as a function of bulk pressure. The results from IAST and work by Tan[5,6] are in good agreement with the simulated results obtained on the basis of the proposed model.

E. Methanol-water mixtures

The variation of dipole moment in the pore as the operating pressure increases are shown in Fig. 10. The values are

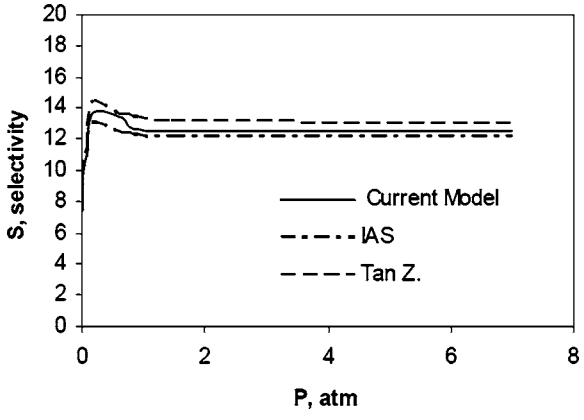

FIG. 9. Comparison of simulated ethane selectivity as a function of operating pressure with the results of Tan *et al.* (Refs. 5 and 6) and results from IAST for pore width of 9.7 Å at $y_{b1}=0.9$ (methane) and $T=286$ K.

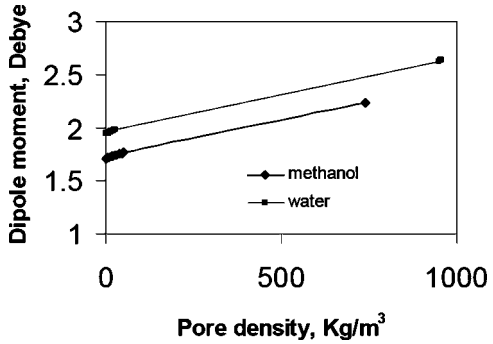

FIG. 10. Variations in dipole moments of methanol and water as a function of their pore densities for a pore width of 30 Å at 298 K with reference to their single component isotherms in Fig. 11.

observed to increase linearly, as discussed in the text. The values of the dipole moments actually used to generate isotherms, shown in Fig. 11, are shown as points in Fig. 10, and depend on the density of the fluid (water or methanol) in the pores.

Figure 11 shows the single component isotherms of methanol and water at 298 K in a 30 Å pore width. Results show that the pore filling in the case of methanol takes place at relatively lower pressure than that of water, due to greater methanol-wall interactions which cause the completion of monolayer formation at low pressure. According to the simulation results of Fileti *et al.*[30] these results imply that the methanol and water are both in vaporlike states before the pore filling, and in a liquidlike state (clusters of dimers) after the pore filling takes place because of hydrogen bonds.

Figure 12 shows the relative magnitudes of fluid-wall (methanol-wall, water-wall) and fluid-fluid (methanol-methanol, water-methanol, and water-water) interactions at 298 K for 15 Å pore width. Before pore filling takes place, the fluid-wall interactions (2–3 kJ/mol) dominate over the fluid-fluid interactions (<0.5 kJ/mol). However, after pore filling, water-water interactions are more significant than other interactions, indicating the preferential adsorption of water due to dipole-dipole (electrostatic) interactions (~10 kJ/mol). Thus, the results imply that the adsorption phenomena is governed by fluid-wall interactions before the

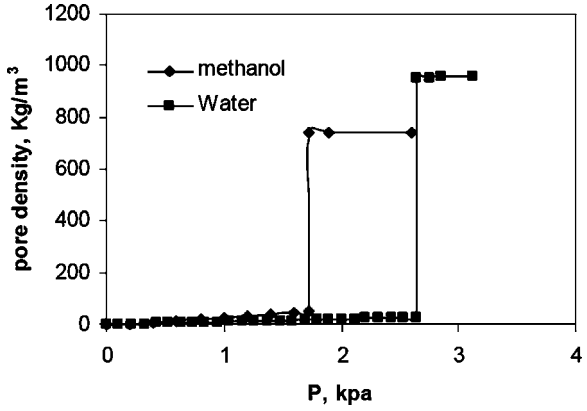

FIG. 11. Single-component pore densities of confined methanol and water as a function of operating pressure for pore width of 30 Å at 298 K.

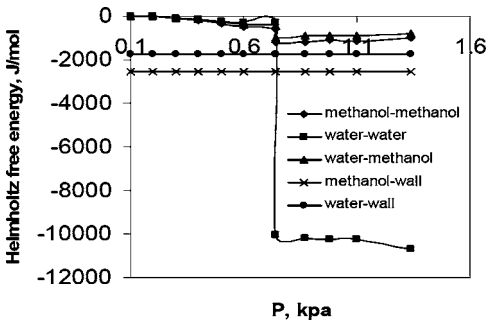

FIG. 12. Relative contributions of methanol-methanol, water-water, water-methanol, methanol-wall, and water-wall interactions in Helmholtz free energy as a function of bulk pressure for 15 Å pore size at $y_{b1}=0.5$ (methanol) and 298 K.

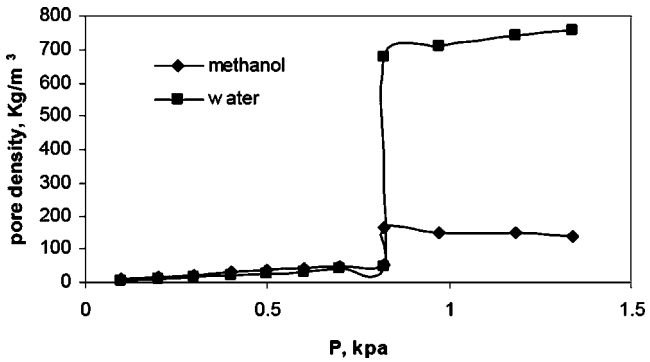

FIG. 14. Pore densities of methanol and water as a function of bulk pressure for 50–50 mole % mixture of methanol-water in 18 Å pore width at 298 K.

pore filling takes place, and by fluid-fluid interactions, mainly water-water interactions, after the pore filling.

Figures 13–15 show the isotherms of a 50–50 mole % of water-methanol mixture for 15, 18, and 25 Å pore sizes. In all cases, before pore filling takes place, methanol adsorbs preferentially over water, because of greater methanol-wall interactions due to the greater polarizability of methanol compared to water. However, once the monolayer forms on the wall, water starts dissolving in methanol and forming clusters through hydrogen bonding with other water molecules. This, in turn, increases the water density in the pores as pressure increases by displacing methanol molecules out of the pore, and implying that the hydrogen bonding between water-methanol and methanol-methanol are less stable than the water-water hydrogen bonds in the pore. The size of the slit-pore relative to the size of adsorbing molecules might be responsible for unstable hydrogen bonds between water-methanol and methanol-methanol. Thus, water adsorbs selectively in the pore after pore filling. The figures also indicate that, as the pore size increases from 15 to 25 Å , the transition pressure for condensation increases due to the larger separation between the interacting walls. Simultaneously, the pore densities of methanol and water decrease before capillary condensation takes place in the pore due to a decrease in fluid-wall interactions. Also, as the pore spacing increases the water and methanol densities at the point of capillary condensation increase due to the increased space available for molecules to participate in hydrogen bonding. However, after capillary condensation, the water density continues to increase with increasing pressure, while the confined methanol density decreases. The stronger hydrogen bonding between water molecules increasingly displaces the methanol out of the pore.

Figure 16 shows the selectivity of methanol over water as a function of operating pressure for pore sizes of 15, 18, and 30 Å . The selectivity of methanol is greater than 1 before the pore filling takes place, due to greater methanol-wall interactions than water-wall interactions, which are attributed to the greater polarizability of methanol molecules. The selectivity is less than 1 after pore filling because water-water interactions are more significant than fluid-wall, methanol-methanol, and methanol-water interactions, as shown in Fig. 12. The figure also indicates that selectivity increases as pore size decreases before the pore filling takes place due to increased methanol-wall interactions before it begins to be displaced.

Figure 17 shows a comparison with the results of Shevade *et al.*[21,22] In order to perform a meaningful comparison, we calculated the saturation pressure of 50% mole fraction of bulk water-methanol mixture using the method described by Schoen *et al.*[23] The following expressions for bulk pressure were used to determine bulk gas-liquid coexistence properties:

$$P = \frac{(\rho_{b1}+\rho_{b2})kT}{(1-\rho_{b1}b_{b1}-\rho_{b2}b_{b2})} - a_{b1}\rho_{b1}^2 - a_{b2}\rho_{b2}^2 - a_{b12}\rho_{b2}^2 \quad (\rho_{b2} < \rho_{b1}), \tag{53}$$

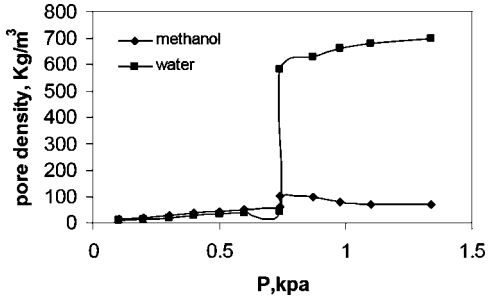

FIG. 13. Pore densities of methanol and water as a function of bulk pressure for 50–50 mole % mixture of methanol-water in 15 Å pore width at 298 K.

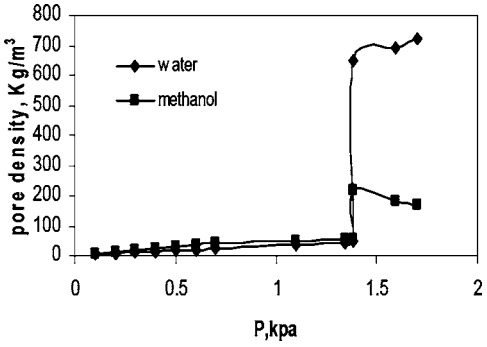

FIG. 15. Pore densities of methanol and water as a function of bulk pressure for 50–50 mole % mixture of methanol-water in 25 Å pore width at 298 K.

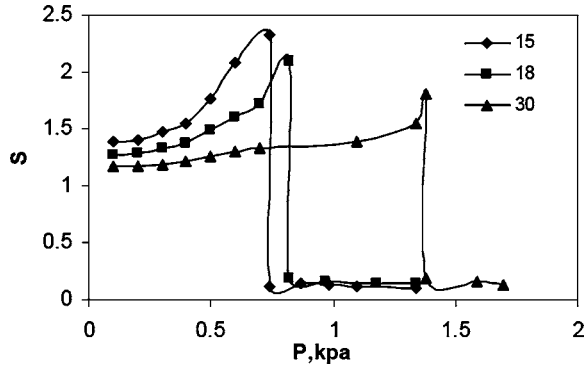

FIG. 16. Selectivities of methanol over water as a function of bulk pressure for $y_{b1}=0.5$ (methanol) at 298 K. Results shown for 15, 18, and 30 Å pore size.

$$P = \frac{(\rho_{b1}+\rho_{b2})kT}{(1-\rho_{b1}b_{b1}-\rho_{b2}b_{b2})} - a_{b1}\rho_{b1}^2 - a_{b2}\rho_{b2}^2 - a_{b12}\rho_{b1}^2 \quad (\rho_{b2} > \rho_{b1}). \tag{54}$$

The bulk saturation pressure was found to be 15.6 kpa. The simulated pore densities of methanol and water and the pore filling pressure deviate somewhat from the values in Shevade *et al.*[21,22] However, the simulated isotherms were qualitatively in agreement with the aforementioned study. It should be pointed out, that additional simulation results based on more advanced, detailed and computationally demanding techniques like GCMC are required in order to further elucidate these deviations.

IV. CONCLUSIONS

The mean-field perturbation theory proposed by Schoen *et al.*[23] and Kotdawala *et al.*[24] was extended to account for binary component mixtures of nonpolar and polar molecules. The theory enabled us to predict the thermodynamic properties of binary mixtures of polar and nonpolar molecules in confined narrow slit-pores. The following conclusions were made:

(1) The adsorption of nonpolar molecules (methane-ethane) is governed by fluid-wall interactions. The selectivity of ethane was found to be more sensitive to pore size than other variables like ethane mole fractions and operating pressure.

(2) The predictions of the selectivity using the proposed model were found in good agreement with the results of Tan and co-workers[5,6] and predictions using IAST.

(3) In the case of methanol-water mixture adsorption, the fluid-wall interactions dominate over fluid-fluid interactions before pore filling takes place. However. the trend reverses after pore filling, resulting in the preferential adsorption of methanol before the pore filling, and preferential adsorption of water after pore filling. The preferential adsorption of methanol before pore filling was attributed to the greater polarizability of the methanol molecule, while the post pore filling phenomena was attributed to the formation of much stronger water-water hydrogen bonds than hydrogen bonds between water-methanol and methanol-methanol molecules.

(4) The usage of angle-averaged dipole-dipole and dipole-induced dipole intermolecular potentials enabled us to predict adsorption isotherms of methanol-water mixture qualitatively. The simulated isotherm of methanol-water mixtures deviated somewhat from the results of Shevade *et al.*[21,22] However, the results were qualitatively similar. In this particular case, sophisticated Monte Carlo simulations are required to further elucidate and comment on the simulated results obtained by using the proposed statistical mechanical model and the mean-field perturbation approach.

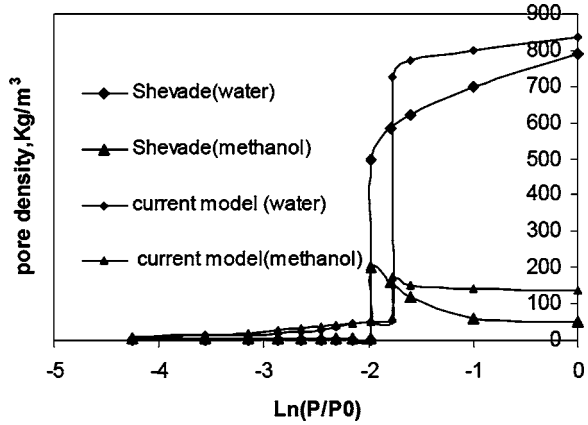

FIG. 17. Comparison of simulated pore densities of methanol and water with the results of Shevade *et al.* (big symbols) as a function of relative pressure for 20 Å pore size at $y_{b1}=0.5$ (methanol) and 298 K.

APPENDIX

Characterization of the terms in Eq. (15). The pore density of component 2 is given by

$$\rho_{p2} = \frac{N_2}{As_z} \tag{A1}$$

with

$$a_{p2} = a_{b2}\left[1 - \left(\frac{\frac{3\sigma_{ff22}}{\sigma_{fw2}}}{4(\xi_2-2)}\right) + \left(\frac{\frac{\sigma_{ff22}^3}{\sigma_{fw2}^3}}{8(\xi_2-2)^3}\right)\right], \tag{A2}$$

$$a_{b2} = \frac{8\pi\varepsilon_{ff22}\sigma_{ff22}^3}{3}, \tag{A3}$$

$$\xi_2 = \frac{s_z}{\sigma_{fw2}}, \tag{A4}$$

$$\sigma_{fw2} = (\sigma_{ff22}\sigma_w)^{1/2}. \tag{A5}$$

Characterization of the terms in Eq. (16),

$$a_{p121} = a_{b121}\left[1 - \left(\frac{\frac{3\sigma_{ff12}}{\sigma_{fw12}}}{4(\xi_1-2)}\right) + \left(\frac{\frac{\sigma_{ff12}^3}{\sigma_{fw12}^3}}{8(\xi_1-2)^3}\right)\right], \tag{A6}$$

$$a_{b121} = \frac{8\pi\varepsilon_{ff12}\sigma_{12}^3}{3}, \tag{A7}$$

$$\varepsilon_{ff12} = (\varepsilon_{ff1}\varepsilon_{ff2})^{1/2}, \tag{A8}$$

$$\sigma_{fw12} = (1/3)(\sigma_{ff11} + \sigma_{ff22} + \sigma_w), \tag{A9}$$

$$\sigma_{ff12} = (1/2)(\sigma_{ff11} + \sigma_{ff22}). \tag{A10}$$

Characterization of the terms in Eq. (24),

$$a_{p22} = \frac{4\pi a_{p2}}{3\sigma_{ff22}^3(s_z - 2\sigma_{fw2})}\left(-\frac{3}{2}\sigma_{ff22} + 2(s_z - 2\sigma_{fw2}) + \frac{\sigma_{ff22}^3}{4(s_z - 2\sigma_{fw2})^2}\right), \tag{A11}$$

$$a_{p2} = \frac{1}{(4\pi\varepsilon_0)^2}\left[\left(\frac{2\mu_2^4}{3kT}\right) + 2\mu_2^2\alpha_2 + \left(\frac{3\alpha_2^2 I_2}{4}\right)\right]. \tag{A12}$$

Characterization of the terms in Eq. (25),

$$a_{p121} = \frac{4\pi a_{p12}}{3\sigma_{ff12}^3(s_z - 2\sigma_{fw12})}\left(-\frac{3}{2}\sigma_{ff12} + 2(s_z - 2\sigma_{fw12}) + \frac{\sigma_{ff12}^3}{4(s_z - 2\sigma_{fw12})^2}\right), \tag{A13}$$

where

$$a_{p12} = \frac{1}{(4\pi\varepsilon_0)^2}\left[\left(\frac{3\alpha_1\alpha_2(I_1 + I_2)}{I_1 I_2 4}\right)\right] + \frac{1}{(4\pi\varepsilon_0)^2}\left(\frac{\mu_1^2\mu_2^2}{3kT} + \mu_1^2\alpha_2 + \mu_2^2\alpha_1\right). \tag{A14}$$

The chemical potentials for components 1 and 2 can be calculated as follows:

$$\left(\frac{\partial F_P}{\partial N_1}\right)_{N_2,T,V} = \mu_{P1}, \tag{A15}$$

$$\left(\frac{\partial F_P}{\partial N_2}\right)_{N_1,T,V} = \mu_{P2}, \tag{A16}$$

$$\left(\frac{\partial F_b}{\partial N_1}\right)_{N_2,T,V} = \mu_{b1}, \tag{A17}$$

$$\left(\frac{\partial F_b}{\partial N_2}\right)_{N_1,T,V} = \mu_{b2}. \tag{A18}$$

The chemical potentials of components 1 and 2 in the pore phase can be calculated as follows:

$$\mu_{P1} = \beta^{-1}\left(\frac{b_{p1}(\rho_{p1} + \rho_{p2})}{(1 - \rho_{p1}b_{p1} - \rho_{p2}b_{p2})} + \ln(1 - \rho_{p1}b_{p1} - \rho_{p2}b_{p2}) - \ln(\rho_{p1}\lambda_1^3)\right) + \psi_1 - 2a_{p1}\rho_{p1} - 2a_{p12}\rho_{p1}, \tag{A19}$$

$$\mu_{P2} = \beta^{-1}\left(\frac{b_{p2}(\rho_{p1} + \rho_{p2})}{(1 - \rho_{p1}b_{p1} - \rho_{p2}b_{p2})} + \ln(1 - \rho_{p1}b_{p1} - \rho_{p2}b_{p2}) - \ln(\rho_{p2}\lambda_2^3)\right) + \psi_2 - 2a_{p2}\rho_{p2}. \tag{A20}$$

The chemical potentials of components 1 and 2 in the bulk phase can be calculated as follows: For $\rho_{b1} < \rho_{b2}$,

$$\mu_{b1} = \beta^{-1}\left(\frac{b_{b1}(\rho_{b1} + \rho_{b2})}{(1 - \rho_{b1}b_{b1} - \rho_{b2}b_{b2})} + \ln(1 - \rho_{b1}b_{b1} - \rho_{b2}b_{b2}) - \ln(\rho_{b1}\lambda_1^3)\right) - 2a_{b1}\rho_{b1} - 2a_{b12}\rho_{b1}, \tag{A21}$$

$$\mu_{b2} = \beta^{-1}\left(\frac{b_{b2}(\rho_{b1} + \rho_{b2})}{(1 - \rho_{b1}b_{b2} - \rho_{b2}b_{b2})} + \ln(1 - \rho_{b1}b_{b1} - \rho_{b2}b_{b2}) - \ln(\rho_{b2}\lambda_2^3)\right) - 2a_{b2}\rho_{b2}, \tag{A22}$$

while for, $\rho_{b2} < \rho_{b1}$,

$$\mu_{b1} = \beta^{-1}\left(\frac{b_{b1}(\rho_{b1} + \rho_{b2})}{(1 - \rho_{b1}b_{b1} - \rho_{b2}b_{b2})} + \ln(1 - \rho_{b1}b_{b1} - \rho_{b2}b_{b2}) - \ln(\rho_{b1}\lambda_1^3)\right) - 2a_{b1}\rho_{b1}, \tag{A23}$$

$$\mu_{b2} = \beta^{-1}\left(\frac{b_{b2}(\rho_{b1} + \rho_{b2})}{(1 - \rho_{b1}b_{b2} - \rho_{b2}b_{b2})} + \ln(1 - \rho_{b1}b_{b1} - \rho_{b2}b_{b2}) - \ln(\rho_{b2}\lambda_2^3)\right) - 2a_{b2}\rho_{b2} - 2a_{b12}\rho_{b2}. \tag{A24}$$

[1] T. Nakahara, M. Hirata, and S. Komatsu, J. Chem. Eng. Data **26**, 161 (1981).
[2] R. J. Grant and M. Manes, Ind. Eng. Chem. Fundam. **5**,490 (1966).
[3] L. Szepesy and V. Illes, Acta Chim. Acad. Sci. Hung. **35**, 245 (1963).
[4] R. Reich, W. T. Ziegler, and K. A. Rogers, Ind. Eng. Chem. Process Des. Dev. **19**, 336 (1980).
[5] Z. Tan, Ph.D. thesis, 1991.
[6] Z. Tan, and K. E. Gubbins, J. Phys. Chem. **96**, 845 (1992).
[7] S. Jiang, K. E. Gubbins, and P. B. Balbuena, J. Phys. Chem. **98**, 2403 (1994).
[8] H. Pan, J. A. Ritter, and P. B. Balbuena, Langmuir **15**, 4570 (1999).
[9] R. F. Cracknell, D. Nicholson, and N. Quirke, in *Molecular Simulation and Industrial Applications Methods, Examples and Prospects*, edited by K. E. Gubbins and N. Quirke (G&B Science Publishers, New York, 1996).
[10] R. F. Cracknell, D. Nicholson, and N. Quirke, Mol. Phys. **80**, 885 (1993).
[11] G. M. Davies and N. A. Seaton, AIChE J. **46**, 1753 (2000).
[12] V. Gun'ko and T. J. Bandosz, Phys. Chem. Chem. Phys. **5**, 2096 (2003).
[13] D. V. Baelen, B. V. D. Bruggen, K. V. D. Dungen, and J. D. C. Vandecasteele, Chem. Eng. Sci. **60**, 1583 (2005).
[14] N. H. Jalani, P. Choi, and R. Datta, J. Membr. Sci. (to be published).
[15] N. H. Jalani, P. Choi, and R. Datta, Solid State Ionics **175**, 815 (2004).
[16] C. Gates and J. Newman, AIChE J. **46**, 2076 (2004).
[17] B. Smitha, S. Sridher, and A. A. Khan, J. Membr. Sci. **225**, 63 (2003).
[18] S. M. Taqvi, W. S. Appel, and M. D. Levan, Ind. Eng. Chem. Res. **38**, 240 (1999).
[19] M. J. D. Linders, L. J. P. van den Broeke, F. Kapteijn, J. A. Moulijn, and J. J. G. M. van Bokhoven, AIChE J. **47**, 1885 (2001).
[20] S. Hietala, S. L. Maunu, and F. Sundholm, J. Polym. Sci., Part B: Polym. Phys. **38**, 3277 (2000).
[21] A. V. Shevade, S. Jiang, and K. E. Gubbins, Mol. Phys. **97**, 1139 (1999).

[22] A. V. Shevade, S. Jiang, and K. E. Gubbins, J. Chem. Phys. **113**, 6933 (2000).
[23] M. Schoen and D. J. Diestler, J. Chem. Phys. **109**, 5596 (1998).
[24] R. R. Kotdawala, N. Kazantzis, and R. W. Thompson, J. Math. Chem. **38**, 333 (2005).
[25] D. Nicholson and K. E. Gubbins, J. Chem. Phys. **104**, 8126 (1996).
[26] T. M. Reed and K. E. Gubbins, *Applied Statistical Mechanics* (McGraw Hill, New York, 1973).
[27] J. M. Smith, H. C. Van Ness, and M. M. Abbott, *Introduction to Chemical Engineering Thermodynamics*, 5th ed. (McGraw Hill, New York, 1996), Chap. 3.
[28] J. M. Prausnitz, R. N. Lichtenthaler, and E. Gomes de Azevedo, *Molecular Thermodynamics of Fluid-Phase Equilibria*, 3rd ed. (Prentice-Hall, New Jersey, 1999).
[29] J. W. Tester and M. Modell, *Thermodynamics and its Applications*, 3rd ed. (Prentice-Hall, New York, 1997).
[30] E. E. Fileti, P. Chaudhuri, and S. Canuto, Chem. Phys. Lett. **400**, 494 (2004).
[31] D. M. Lubman and M. N. Kronlck, Anal. Chem. **55**, 867 (1983).
[32] A. Striolo, A. A. Chialvo, P. T. Cummings, and K. E. Gubbins, Langmuir **19**, 8583 (2003).
[33] A. L. Myers and J. M. Prausnitz, AIChE J. **11**, 121 (1965).
[34] D. P. Valenzuela and A. L. Myers, *Adsorption Equilibrium Data Handbook* (Prentice-Hall, New Jersey, 1989).